Theory of field evaporation of the surface layer in jellium and other metals

Edward R. McMullen* and John P. Perdew
Department of Physics and Quantum Theory Group, Tulane University, New Orleans, Louisiana 70118
(Received 10 February 1987)

An intense, positive electric field applied normal to a metal surface can displace or even strip away the surface layer of atoms. These effects are studied for a jellium model ($r_s = 4.20$ a.u., surface layer thickness $d = 5.65$ a.u.) via fully self-consistent calculations within the local-density approximation for exchange and correlation. From plots of surface energy versus displacement for several fields of interest, the critical field F_c required to evaporate the rigid surface layer is found (1.8 V/Å) and compared with the prediction (1.7 V/Å) of a simple semiempirical formula based upon universal binding-energy curves. The calculations also reveal information about electronic-charge redistribution, electronic resonances which develop with increasing separation of the surface layer from the bulk, and various components of the surface-layer–bulk binding force. The jellium surface is compared with the real-metal surface Na(110) and with Al(111), which was investigated in earlier semi-self-consistent work.

I. INTRODUCTION

Electric field interaction with the metal surface has received increasing theoretical attention in recent years as more powerful methods of analysis have become available. Estimates of field penetration into the metal,[1] induced–surface-charge distribution $\delta n(\mathbf{r})$,[2–5] physical characteristics of $\delta n(\mathbf{r})$ such as the location of the effective charged surface[1,6] and the screening length,[1] field dependency of capacitance,[2] field emission and ionization,[2] field desorption of chemisorbed ions,[7] field-induced surface-layer displacements,[5,8] and field evaporation[8] are in the literature. An instrument which utilizes the direct application of an intense positive electric field to the metal surface is the field-ion microscope.[9] In field-ion microscopy (FIM), positive ions are ripped away from a stepped metal surface by an electric field of several volts per angstrom. The processes involved are complicated and not fully understood. In the present attempt at a microscopic theory of clean-surface field evaporation, the geometry of the problem has been simplified. A Kohn-Sham density-functional[10] calculation has been performed for a *planar* metal surface in the presence of a normal, positive electric field. With the subsurface ion layers frozen, the field has been increased up to a critical value at which the entire surface lattice plane is stripped away. What emerges is a detailed picture of the microscopic forces acting upon the surface layer, its equilibrium displacement from the bulk as a function of field, the distribution of electronic charge, and the formation of electronic resonances in the surface layer as it separates from the bulk.

In a preliminary report of our work,[8] we presented the results of a variational self-consistent calculation for field evaporation of the Al(111) surface, in which the three-dimensional electron-density profile near the surface was approximated by an optimized one-dimensional profile. Based upon those results, a simple semiempirical formula for the critical field was proposed and applied to many other metal surfaces. Necessarily, those earlier microscopic calculations were not fully self-consistent, and they were also beset by numerical instabilities that limited the range of surface-layer–bulk separations which could be studied. Thus in the present paper we shall study the jellium model of the metal surface, for which fully self-consistent and numerically stable solutions have been found for all separations and field strengths of interest. In the jellium model, the bulk lattice of ions is replaced by a rigid semi-infinite uniform positive background of density $\bar{n} = 3/4\pi r_s^3$, and the surface lattice plane is replaced by a movable "slice" of this background with thickness d. We believe that the present study is the first fully self-consistent Kohn-Sham[10] calculation of field evaporation. The results confirm and extend our earlier conclusions about the physical processes involved and the reliability of the semiempirical formula.

II. THE MODEL

The metal surface model to be employed in this work has been developed in several previous papers[3,4,11] and is reviewed in Ref. 8. The density-functional theory[10] of the inhomogeneous electron gas is a ground-state theory in which total surface energy is divided into noninteracting kinetic and exchange-correlation energies, σ_s and σ_{xc} respectively, and electrostatic energy σ_{es} of that gas and the positive background charge distribution of the crystal, which we take to occupy the half-space $x < 0$. In the case of jellium, the background charge is uniform; for real metals, the ionic structure of the crystal must be taken into account. Calculations within density-functional theory are usually self-consistent in the electron density and potentials, as they are in the present work. All physical ground-state information about the crystal may be deduced from the electronic and positive background charge densities.

In practice, the input potential to the first iteration is adjusted to reflect both a shift of the surface ion layer out of registry by a displacement λd normal to the sur-

face (where λ is a dimensionless displacement parameter), and an externally applied electric field F which induces a positive surface charge $\Sigma = F/4\pi$ (esu) in the metal. The Kohn-Sham[10] (KS) equations are solved for this trial potential, and a density $n(x,\lambda,F)$ is constructed from the KS orbitals. This density yields a new potential. The process is iterated to self-consistency. Solutions thus obtained are subject to several well-known constraints such as overall charge conservation in the system, satisfaction of the Sugiyama-Langreth[12] sum rule for the phase angles obtained in solving the KS equations, and agreement between the change in electrostatic potential and the dipole moment across the surface. In this manner, a mapping of surface energy σ versus layer displacement λd may be constructed for a given field. Repeating the process for several fields over a range of interest produces a family of self-consistent σ versus λ curves (see Fig. 1 of Ref. 8, for example). Electron-density profiles obtained for a particular λ and for zero and nonzero F yield the density profile of the field-induced charge δn, its charge center $\bar{x}$, and therefore the effective electrical surface of the metal for a particular F and λ.

In our work, exchange-correlation energies were calculated within the commonly used local-density approximation using an interpolation formula[13]

$$\varepsilon_{xc}(n) = Ar_s^{-1} + B(1 + Cr_s^{1/2} + Dr_s)^{-1} \quad (1)$$

from the work of Ceperley and Alder.[14] The most-dense faces of the two metals considered were selected for study under the assumption that intraplanar forces would be greatest for these faces (i.e., surface reconstruction would be least) and interplanar forces would be weakest between these layers (i.e., the critical field F_c for surface-layer evaporation would be smallest).

The bulk energy of jellium is stable at $r_s = 4.20$ a.u. when the exchange-correlation energy per particle is given by Eq. (1). Of the simple metals, Na ($r_s = 3.93$ a.u.) has its bulk electronic density closest to this value. The densest lattice plane of the bcc structure of Na is (110), with a bulk interplanar spacing $d = 5.65$ a.u. We thus chose $r_s = 4.20$ a.u. and a surface-layer thickness $d = 5.65$ a.u. for our jellium metal. We will refer to this metal as sodium-jellium, or "NaJ."

III. SURFACE ENERGIES AND SURFACE-LAYER–BULK BINDING FORCES

Fully self-consistent NaJ surface energies have been calculated for a broad range of surface-layer displacements λd and externally applied fields F. For $F = 0$ the data may be graphically presented in a σ versus λ format. When several curves for different field strengths are to be plotted, $\Delta\sigma$ versus λ is more convenient, where $\Delta\sigma = \sigma(\lambda,F) - \sigma(0,F)$ is the surface energy variation with λ for a given field. Self-consistent $\Delta\sigma$ versus λ curves for NaJ, $-0.05 \le \lambda \le 0.50$, and $F = 0.00$, 1.00, 1.80, and 2.00 V/Å, are shown in Fig. 1. The $F = 1.80$ V/Å curve displays the characteristics associated with the onset of field evaporation and identifies the critical field for NaJ as $F_c = 1.8$ V/Å.

Figure 2 displays, for $F = 0.00$ V/Å, the total surface

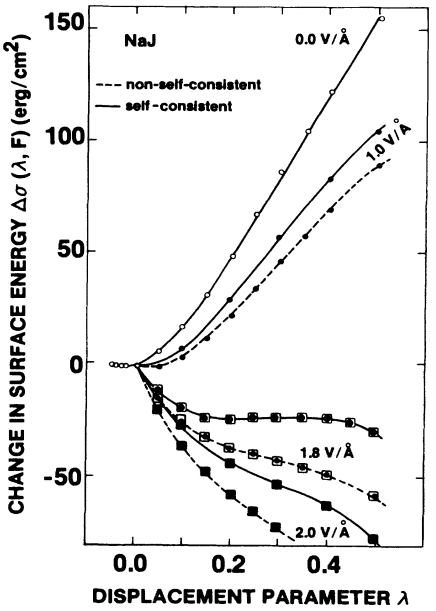

FIG. 1. Change in surface energy σ versus surface-layer displacement λd for the self-consistent sodium-jellium (NaJ) calculations and the non-self-consistent model of Eq. (6). The parameters α and β of the non-self-consistent model are the "best-fit" values from Table VI.

energy σ and its components σ_s, σ_{es}, and σ_{xc}. Let $x_\lambda = \lambda d$. It can be seen from the shapes of the curves that, while the surface-layer–bulk forces $f = -\partial\sigma/\partial x_\lambda$ are everywhere attractive for $\lambda > 0$, the component forces $f_i = -\partial\sigma_i/\partial x_\lambda$ are not. The kinetic-energy (σ_s) forces strongly favor separation of the surface layer from the

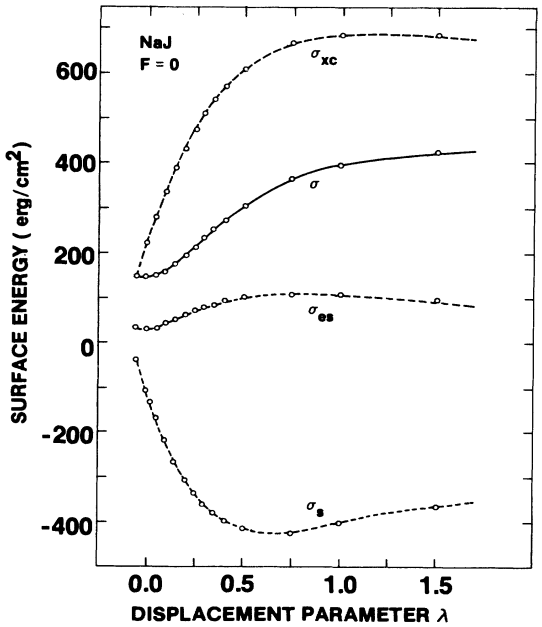

FIG. 2. The NaJ zero-field self-consistent energy curve (solid line) and its components, kinetic (σ_s), electrostatic (σ_{es}), and exchange-correlation (σ_{xc}) (dashed lines).

bulk for small λ ($0<\lambda<0.25$), weaken ($0.25<\lambda<0.70$), and turn moderately attractive for $\lambda>0.70$. The opposite is true for σ_{xc}, which at first strongly favors binding ($0<\lambda<0.60$), weakens ($0.60<\lambda<1.10$), and turns moderately repulsive. Indeed σ_s and σ_{xc} largely neutralize each other. The small-λ dependence of the total surface energy is controlled by that of the electrostatic component σ_{es}, as predicted by the Hellmann-Feynman theorem.[15] σ_{es} shows moderate forces in comparison with σ_s or σ_{xc}, initially favoring binding ($\lambda<0.60$) and then becoming weakly repulsive ($\lambda>0.60$). Estimates of the relative strengths of these forces made from the slopes of the curves in Fig. 2 are presented in Table I. The shapes of the component binding-energy curves are similar to those of a diatomic molecule as discussed by Levine[15] from the point of view of the quantum-mechanical virial theorem.

A plot of $\Delta\sigma_i$ (components of the change in surface energy) versus surface-layer displacement for $F=0.00$ and $F=F_c$ is presented in Fig. 3. Quite clearly, the field dependencies of $\Delta\sigma_s(\lambda,F)$ and $\Delta\sigma_{xc}(\lambda,F)$ are opposed to each other and individually are much smaller than those of $\Delta\sigma(\lambda,F)$ and $\Delta\sigma_{es}(\lambda,F)$. If the kinetic and exchange-correlation contributions to $\Delta\sigma(\lambda,F)$ are added, $\Delta\sigma_{sxc}(\lambda,F)=\Delta\sigma_s(\lambda,F)+\Delta\sigma_{xc}(\lambda,F)$ remains remarkably insensitive to F over $0<F<2.00$ V/Å, accounting for less than 5% of the field dependence of $\Delta\sigma$. Evidently the field dependence of the surface energy at any layer displacement is predominantly electrostatic in nature, as it would be in the weak-field limit.

IV. ELECTRONIC CHARGE DISTRIBUTION

The electron gas is fluid and responds to both surface-layer displacement and applied field. Over the ranges of our calculations for NaJ, $0<\lambda<1.50$, $0<F<2.00$ V/Å, the behavior of such quantities as the number of electrons per unit area associated with the surface layer and the location of the effective metallic surface may be investigated.

Figure 4 displays self-consistent electron-density profiles for several surface-layer separations and $F=0.00$ V/Å. Separation of the profiles into two distinct regions associated with the surface layer and the bulk is clear. For emphasis, the $\lambda=0$ and ∞ electron profiles are superimposed to show their development with increasing λ. Note that, at $\lambda=1.50$, several separation-dependent quantities are within a few percent of their asymptotic values ($\lambda=\infty$) as indicated by the data in Table II. In that table, x_{min} is the location of the minimum in the density profile which develops between the nominal bulk surface at $x=-d$ and the trailing edge of the surface-layer background charge at $x=(\lambda-1)d$, and

$$Q_\lambda=\int_{x_{min}}^{\infty} dx\, n(x,\lambda,F) \tag{2}$$

is the number of electrons per unit area between x_{min} and ∞. Q_λ does not count electrons removed from the metal surface by the nonzero field that generates the surface charge.

Self-consistent densities for $F=0.00$ and 2.00 V/Å, $\lambda=0.20$, are shown in Fig. 5, which also includes the induced surface charge density δn. The centroid of induced surface charge $\bar{x}$, taken with respect to the leading edge of the surface-layer background at $x=\lambda d$, is

$$\bar{x}=\Sigma^{-1}\int_{-\infty}^{\infty} dx\,(x-\lambda d)[n(x,\lambda,0)-n(x,\lambda,F)]$$
$$=\Sigma^{-1}\int_{-\infty}^{\infty} dx\,(x-\lambda d)\delta n(x,\lambda,F)\ . \tag{3}$$

In the weak-field limit, this centroid is just the position of the classical "image plane." Calculated centroids are presented in Table III. Note that (a) for all λ, an increase in field drives the centroid into the surface layer as expected, (b) for a particular field, the centroid variation with λ is confined to a small interval of no more than 0.13 a.u. for the fields considered, and (c) with increasing λ, the centroids first move outward from the surface layer for smaller λ, and then shift inward for larger surface-layer–bulk separations.

Perhaps the most meaningful information concerning the partitioning of electronic charge between surface layer and bulk is Q_λ of Eq. (2), a count of the electrons per unit area in the surface-layer region (from x_{min} to infinity), which was evaluated for $F=0$ in Table II. An isolated layer in an applied field F should have a total

TABLE I. Estimated surface-layer–bulk total force per unit area (f) and components (f_i) for various displacements (λ) of the surface layer, NaJ, $F=0$. Estimates are from the slopes of curves in Fig. 2. Forces are in units of 10^8 erg/cm^3. Negative forces represent binding between surface layer and bulk. Note that zero-field lattice relaxation at the surface gives $\lambda_0=-0.025$.

λ	f	f_s	f_{es}	f_{xc}
−0.05	17	485	17	−485
−0.025	0	435	0	−435
0.00	−17	400	−17	−400
0.10	−74	350	−57	−368
0.20	−127	234	−54	−308
0.30	−144	134	−54	−224
0.40	−114	87	−33	−167
0.50	−100	43	−27	−117
0.75	−67	−17	0	−50
1.00	−33	−30	3	−7
1.50	−13	−23	3	7

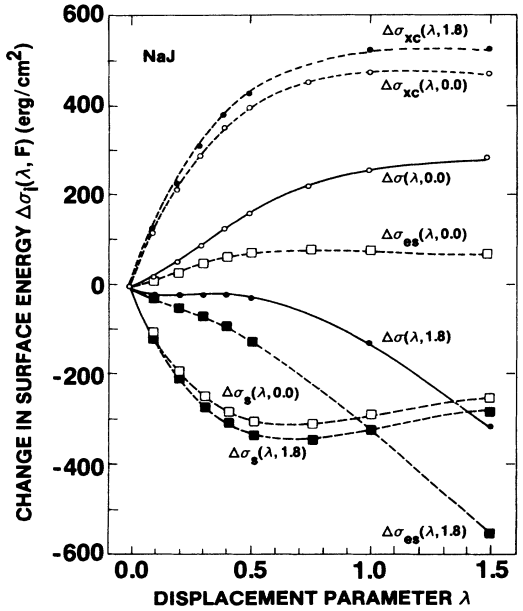

FIG. 3. Change in surface energy versus surface-layer displacement, NaJ, $0 \leq \lambda \leq 1.50$, $F = 0.00$ and 1.80 V/Å. Total surface energy and components are displayed, from which information about the attraction and/or repulsion forces can be obtained.

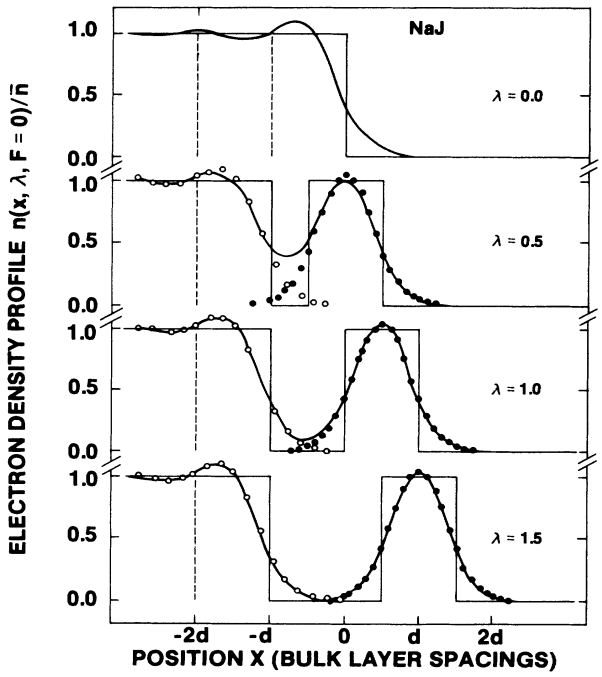

FIG. 4. Sodium-jellium (NaJ) electron-density profiles for $F = 0$ and $\lambda = 0.00$, 0.50, 1.00, and 1.50. Superimposed on the $\lambda > 0$ curves are the $\lambda = 0$ electron-density profile (open circles) and the isolated surface-layer profile (solid circles) appropriately shifted for comparison. Thin lines are $n_+(x)/\bar{n}$, thick lines are $n(x)/\bar{n}$.

TABLE II. Some data pertinent to zero-field separation of the surface layer of NaJ from the bulk. Refer to the text for a description of quantities in the column headings. These data correlate with the charge density profiles in Fig. 4.

λ	$\frac{n(x_{\min})}{\bar{n}}$	$\frac{Q_\lambda}{\bar{n}d}$	$\frac{\Delta\sigma(\lambda,0)}{\Delta\sigma(\infty,0)}$
0.50	0.383	1.021	0.55
1.00	0.112	1.010	0.89
1.50	0.027	1.006	0.98
∞	0.000	1.000	1.00

electron count of $Q_\infty A = (\bar{n}d - \Sigma)A$. Then $Q_\lambda/Q_\infty = Q_\lambda/(\bar{n}d - \Sigma)$ is the ratio of actual to asymptotic electron number associated with the surface layer. This quantity (see Table IV) decreases with increasing λ for all F, asymptotically approaching unity as expected. Thus, in NaJ, some electronic charge drains from the surface layer to the bulk for increasing λ.

V. ELECTRONIC RESONANCES IN THE SEPARATING LAYER

As surface-layer–bulk separation increases, one or more resonances in the Kohn-Sham orbitals ψ_k (which generate the electron density) develop at particular wave vector components k_r normal to the surface. The phenomenon of resonances is well known in the study of thin films,[16] which are usually several layers thick and are completely isolated from other systems. A single resonance in our two-component system should approach a predictable value as λ increases. Consider a separated slice of jellium in the yz plane, width d, and cross section A. The number of electron states allowed in this slice, assuming it can support only one discrete wave vector com-

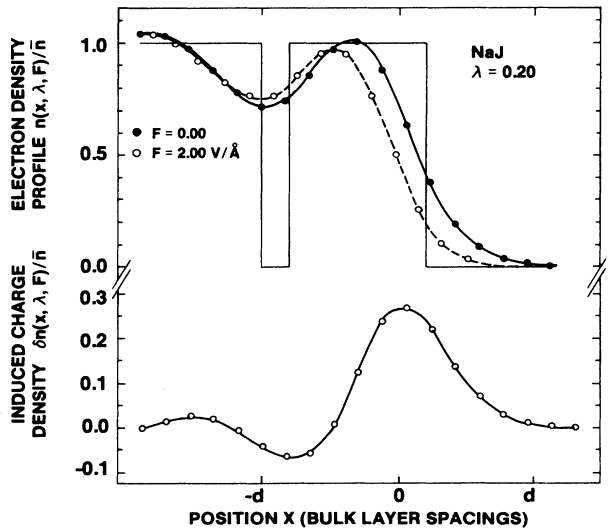

FIG. 5. Electron-density profiles (upper section) for $F = 0.00$ and 2.00 V/Å and induced charge density $\delta n(x, \lambda, F)$ (lower section), NaJ, $\lambda = 0.20$. $\delta n(x, \lambda, F)$ is the difference between the two profiles of the upper section.

TABLE III. NaJ centroids $\bar{x}(\lambda,F)$ of induced surface charge, with respect to the leading edge of the displaced surface layer of background charge at $x=\lambda d$. F is in V/Å and the $\bar{x}$'s are in a.u.

			$\bar{x}$		
λ	$F=0.010$	$F=0.10$	$F=1.00$	$F=1.80$	$F=2.00$
0.00	1.37	1.055	0.41	0.023	−0.059
0.10			0.47	0.082	−0.0030
0.20			0.50	0.12	0.039
0.30			0.50	0.14	0.059
0.40			0.49	0.14	0.066
0.50			0.47	0.13	0.062
1.00				0.083	
1.50				0.021	

ponent k_r parallel to the x axis, is

$$N=2\sum_{\mathbf{k}_{\rm occ}}1=2(A/4\pi^2)\int_0^{(k_F^2-k_r^2)^{1/2}}dk_{yz}\,2\pi k_{yz}$$
$$=(A\varepsilon_F/\pi)(1-k_r^2/k_F^2)\ , \tag{4}$$

where k_F is the Fermi wave vector, $\varepsilon_F=k_F^2/2$, and k_{yz} is the yz component of $\mathbf{k}_{\rm occ}$. Now this number must approach $\bar{n}dA-\Sigma A$ for large λ, where $\bar{n}=k_F^3/3\pi^2$ is the bulk electron density. Thus, in the limit as λ approaches infinity, we obtain

$$k_r/k_F=(1-2k_Fd/3\pi+\pi\Sigma/\varepsilon_F)^{1/2}\ . \tag{5}$$

Table V gives self-consistent resonant wave vectors k_r for several finite values of λ, showing how, with increasing separation, the resonant wave vector approaches the value predicted by Eq. (5). Self-consistent k_r for finite λ were determined as follows: In the bulk metal interior far from the surface region, electronic wave functions of the form

$$\psi_{\mathbf{k}}(\mathbf{r})=\sin(kx-\gamma_k)\exp[i(k_yy+k_zz)]$$

are expected, where $\mathbf{k}=(k,k_y,k_z)$ and $\mathbf{r}=(x,y,z)$. γ_k is a wave-vector-dependent phase angle which must be zero at $k=0$ and continuous over k.[12] For $\lambda=0$, γ_k increases monotonically over the range $0\le k\le k_F$. For $\lambda>0$, γ_k is found to be negative for small k and positive for $k\to k_F$, passing through a zero at what we identify as the resonance $k=k_r$. The transition of γ_k from negative to positive for $\lambda>0$ occurs in a zone of width Δk approximately centered on k_r. Although the width of this zone is difficult to measure precisely, our calculations show conclusively that $\Delta k\to 0$ as $\lambda\to\infty$ (i.e., γ_k becomes discontinuous at k_r), as expected.

VI. SEMIEMPIRICAL FORMULA FOR THE CRITICAL FIELD

Binding-energy curves for diverse systems display nearly universal behavior.[17] In previous work,[8] the universal binding-energy curve was used to generate non-self-consistent (NSC), field-dependent $\Delta\sigma$ versus λ curves for the metal surface. This model parametrizes $\Delta\sigma(\lambda,F=0)$ via two physical quantities: the energy α required to completely separate the surface layer from equilibrium, and a scaling length l. The remarkable fit of our self-consistent Al(111) and NaJ zero-field energies to the universal binding-energy curve is shown in Fig. 6. For nonzero fields, an additional term approximates the correction to $\Delta\sigma(\lambda,F=0)$ arising from surface-layer displacement in the presence of the field:

$$\Delta\sigma^{\rm NSC}(\lambda,F)=\alpha[(1+\beta_0)\exp(-\beta_0)-(1+\beta_\lambda)\exp(-\beta_\lambda)]$$
$$-(F^2/8\pi)\lambda d\ , \tag{6}$$

where $\beta_\lambda=(\lambda-\lambda_0)d/l$ and λ_0 is the equilibrium displacement in the absence of the field. The last term in Eq. (6) is a simplification of the weak-field limit $-(F^2/8\pi)(\lambda d+\bar{x}_\lambda-\bar{x}_0)$, which takes into account the weak λ

TABLE IV. Relative electronic charge Q_λ/Q_∞ associated with the displaced surface layer for the NaJ metal. $Q_\lambda=\int_{x_{\rm min}}^{a}dx\,n(x,\lambda,F)$ is the total effective surface-layer electronic number and $Q_\infty=\bar{n}d-\Sigma$ is the asymptotic surface-layer electronic number (per unit area). F is in V/Å.

			Q_λ/Q_∞	
λ	$F=0.00$	$F=1.00$	$F=1.80$	$F=2.00$
0.10	1.11	1.18	1.25	1.26
0.20	1.06	1.09	1.12	1.12
0.30	1.04	1.06	1.08	1.08
0.40	1.03	1.04	1.05	1.06
0.50	1.02	1.03	1.05	1.05
1.00	1.01		1.02	
1.50	1.01		1.01	

TABLE V. NaJ self-consistent and predicted ($\lambda=\infty$) critical resonances k_r/k_F. The fields F are in V/Å. Predicted values of k_r/k_F are from Eq. (5).

	k_r/k_F			
F	$\lambda=0.50$	1.00	1.50	Predicted ($\lambda\rightarrow\infty$)
0.00	0.651	0.667	0.671	0.672
1.00	0.679			0.706
1.80	0.701	0.722	0.727	0.732
2.00	0.707			0.738

dependence of the centroid $\bar{x}$. The parameters α and l may be determined from a fit of the universal binding-energy curve to the self-consistently calculated zero-field curve $\Delta\sigma(\lambda,F=0)$. Alternatively, these parameters may be estimated empirically: the parameter α is roughly twice the surface energy (an approximation which becomes exact at large d), and the scaling length l may be estimated from the bulk-phonon spectrum for wave vectors normal to the surface. Reference 8 contains estimates of the critical field for the onset of field evaporation of the surface layer for several real metals. The model predicts critical fields higher by 70–140 % than those obtained by field ion microscopy studies wherein a single atom or ion is removed from a needle-shaped metal sample with a typical radius of several hundred Å at the tip.

For NaJ, the NSC energies generated by Eq. (6) (see Fig. 1) are lower than the calculated self-consistent energies, although the λ variations are similar. The NSC curves imply a critical field of 1.7 V/Å, only 0.1 V/Å less than F_c from the self-consistent $\Delta\sigma$ versus λ.

A general expression for F_c may be obtained from Eq. (6) by imposing the condition that at the critical field, the minimum in $\Delta\sigma$ versus λ for $F<F_c$ just disappears and becomes coincident with the inflection point. The expression is

$$F_c^{\mathrm{NSC}}=2(2\pi\alpha/el)^{1/2}\ , \tag{7}$$

where e is the base of natural logarithms. The scaling length l may be estimated in a number of ways. Rose *et al.*[17(d)] have expressed l in terms of an elastic constant C_{11} appropriate to strain normal to the surface,

$$l_s=(\alpha d/C_{11})^{1/2}\ . \tag{8}$$

Bulk phonon dispersion curves lead to the l_{th} of McMullen *et al.*[8] From self-consistent energies, the scaling length may be determined in several ways: l_{BF} from the "best fit" (in the sense of least squares) of SC data to the universal binding energy curve, l_{SL} from the slope at the point of inflection ($\lambda=\lambda_c$ and $\beta_\lambda=1$) of $\Delta\sigma(\lambda,0)$, and l_{SD} from the second derivative evaluated at $\lambda=\lambda_0$. Expressions for l_{SL} and l_{SD} are

$$l_{\mathrm{SL}}=(\alpha d/e)/(\partial\sigma(\lambda,0)/\partial\lambda\,|_{\lambda=\lambda_c})\ , \tag{9}$$

$$l_{\mathrm{SD}}=d\,(\alpha/\partial^2\sigma(\lambda,0)/\partial\lambda^2\,|_{\lambda=\lambda_0})^{1/2}\ , \tag{10}$$

again, where e is the base of natural logarithms. Of the various methods for obtaining the screening length, the one which showed most satisfactory agreement with l_{BF} was l_{SL}, with less than 2% difference for both NaJ and Al(111) (see Table VI).

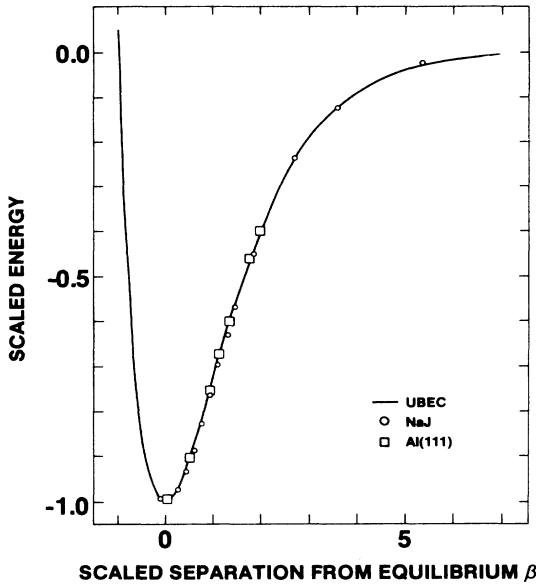

FIG. 6. The universal binding-energy curve (UBEC). Shown also are the scaled, calculated values of surface energy for the NaJ and Al(111) surfaces using $l=l_{\mathrm{BF}}$ (from Table VI).

We are now in a position to calculate critical fields for the onset of field evaporation via Eq. (7) from both experimental data and SC calculations. l_s, l_{th}, and α are quantities whose values may be calculated from experimental data, whereas l_{BF}, l_{SL}, l_{SD}, and α_{SC} are obtained from the self-consistent $\Delta\sigma$ versus λ zero-field calculation. Jellium metals are fictitious; however, the bulk-phonon spectrum of a jellium metal may be calculated from an expression derived in the Appendix, and from this l_{th} may be determined. The bulk-phonon spectra for NaJ and Na(110) are presented for comparison in Fig. 7. Predicted critical field strengths via Eq. (7) from both experimental and SC information are presented in Table VI. The results are rather insensitive to the choice of input parameters α and l. Table VI also shows that approximating α by twice the surface energy $\sigma(\lambda_0,F=0)$ is justified for NaJ.

VII. COMPARISON OF NaJ AND Al(111)

Up to this point, we have presented results of our calculations on the NaJ metal with its uniform background of positive charge; we now compare those to results obtained from a previous calculation[8] on the Al(111) surface, with the ionic lattice modeled via pseudopotential theory.

The shapes of the SC $\Delta\sigma$ versus λ curves for both metals are very similar. Both NaJ and Al(111) zero-field curves display an equilibrium (at $\lambda=\lambda_0$) and a monotonic rise in $\Delta\sigma$ with λ through an inflection point. An asymptotic approach to a limiting energy for $\lambda\rightarrow\infty$ is evident for NaJ; the real-metal calculation was not extended beyond $\lambda=0.50$ for any applied field strength F.

TABLE VI. Estimates of the critical field for the onset of field evaporation from Eq. (7) for Na*J* and Al(111). Scaling parameters l are estimated by various methods as discussed in the text.

Surface	Scaling parameter l (Å)	α (erg/cm^2)	F_c^{NSC} (V/Å)
Al(111)	$l_s=0.66$[a]	2280[b]	5.4
	$l_{th}=0.62$[b]	2280	5.5
	$l_{BF}=0.55$	1490[c]	4.7
	$l_{SL}=0.54$	1490	4.7
	$l_{SD}=0.54$	1490	4.7
Na*J*	$l_{th}=0.77$	285[c]	1.8
	$l_{BF}=0.85$	294[d]	1.7
	$l_{SL}=0.84$	294	1.7
	$l_{SD}=1.0$	294	1.6
Na(110)	$l_{th}=1.1$[b]	522[b]	2.0

[a] Reference 17(d).
[b] Reference 8.
[c] From the approximation $\alpha=2\sigma^{SC}(\lambda_0, F=0)$.
[d] From $\alpha=\sigma^{SC}(\infty,0)-\sigma^{SC}(\lambda_0,0)$.

Both sets of curves show movement of the energy minimum toward the inflection point (at $\lambda=\lambda_c$) with increasing F, and disappearance of this minimum altogether for $F>F_c$; all the curves are monotonically decreasing for $\lambda>0$ and $F>F_c$.

The NSC sets of curves generated by Eq. (6) are shaped like the corresponding SC curves, but the NSC curves for a given field strength and separation are somewhat lower than their SC counterparts for Na*J* (see Fig. 1) and somewhat higher for Al(111) (see Fig. 1 of Ref. 8). Thus the predicted F_c via the NSC curves are different from the F_c^{SC}, but only by an estimated one or two tenths of a volt per angstrom in either case.

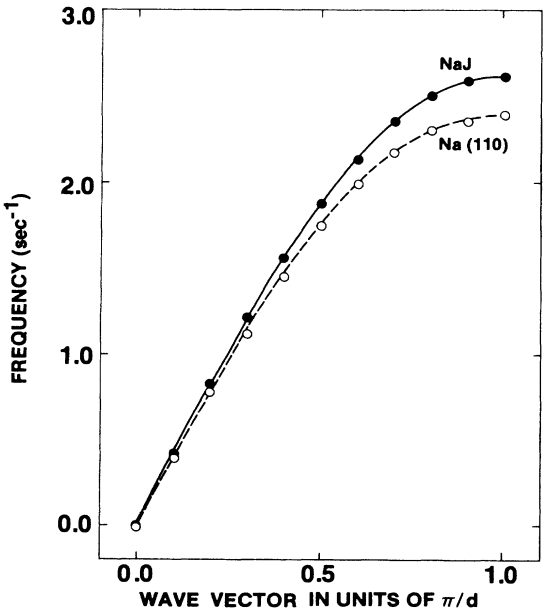

FIG. 7. Na*J* longitudinal phonon frequencies from the Appendix. For comparison, the longitudinal phonon frequencies for Na(110) from Ref. 21 are shown.

Both Na*J* and Al(111) show that the greatest field dependency of $\Delta\sigma$ arises from the term $\Delta\sigma_{es}$, with proportionately very small changes in $\Delta\sigma_s$ and $\Delta\sigma_{xc}$ over the ranges of F considered. [For Al(111), $\Delta\sigma_{es}$ includes discrete-lattice contributions.]

Electronic charge drains from the bulk to the surface layer as separation increases for Al(111), in the direction opposite that for Na*J*. The centroid ($\bar{x}$) of the induced charge for a given field is a monotonically decreasing function of λ in Al(111), unlike the more complicated behavior found in Na*J*. Also, the field dependence of $\bar{x}$ is less pronounced in Al(111) than in Na*J*.

VIII. DISCUSSION AND CONCLUSIONS

In our work on the field evaporation of the jellium surface, we have employed the self-consistent one-dimensional model developed by Lang and Kohn.[3] For real metals, we have adopted the modifications of this model by Monnier and Perdew.[4,11] The topics of resonance development for increasing separation between surface layer and bulk, charge draining, centroid shifts, force components, and field dependence of these properties have been explored. Additionally, methods for calculating the jellium bulk-phonon dispersion curve and the large-displacement resonant wave vector in the surface layer have been presented. A simple non-self-consistent (NSC) model for predicting the onset of field evaporation, either from experimental data or from zero-field self-consistent calculations, has been developed and tested.

Estimates of F_c via self-consistent curves ($F_c^{SC}=4.5$ V/Å for Al(111), 1.8 V/Å for Na*J*) and via the NSC formula of Eq. (7) using self-consistent zero-field data ($F_c^{NSC}=4.7$ V/Å for Al(111), 1.7 V/Å for Na*J*) are in good agreement. F_c^{NSC} from experimental data for Al(111) yields a higher critical field (5.5 V/Å) than F_c^{SC} by about 20%. The source of this 20% discrepancy is presumably the error of the local-density approximation, which underestimates the exchange-correlation contribution to the surface energy. For Na(110), the real-metal

surface closest to NaJ, $F_c^{\rm NSC}$ from experimental data is 2.0 V/Å, while the result for NaJ, using the phonon spectrum of Fig. 7, is 1.8 V/Å. Reference 8 compares $F_c^{\rm NSC}$ from experimental data and $F_c^{\rm FIM}$ from field ion microscopy for several metals. FIM results are considerably lower in all cases for which information is available. This is probably because our work is for the rigid surface layer, while FIM involves fields applied to sharply rounded samples from which individual atoms or ions are removed at exposed sites on the surface. The image-hump model[9] treats field evaporation of individual ions from the nonplanar metal surface. This theory predicts critical fields in generally good agreement with those observed in FIM. However, the critical field of 1.9 V/Å predicted[9] for Al by this theory is considerably lower than the FIM value of 3.3 V/Å for Al(111).

For the critical field needed to strip a rigid surface layer from a rigid bulk, we conclude that our earlier NSC estimates for real metals using experimental data are essentially correct. The NSC model is based upon two assumptions: (a) the zero-field curves $\Delta\sigma(\lambda, F=0)$ for metals scale onto a universal binding energy curve, and (b) the field-dependent term in $\Delta\sigma(\lambda,F)$ is $-(F^2/8\pi)\lambda d$. For both NaJ and Al(111), we have verified the accuracy of assumption (a). We have found that assumption (b) is good enough for the estimation of the critical field, but less reliable than assumption (a). While the field dependence of $\Delta\sigma(\lambda,F)$ arises predominantly from that of the electrostatic term $\Delta\sigma_{\rm es}$, the weak-field expression for this dependence is not entirely appropriate for the intense fields considered here.

Several other studies have dealt with zero-field surface layer relaxation[18] and/or the interaction of the metal surface with a strong external field.[5–8] In particular, we cite two which appeared after our work on Al(111) field evaporation: (1) Kiejna[5] has performed analytical calculations of field-induced surface-layer displacements in the metals Li, Na, Cu, and Al under the influence of negative fields up to 0.5 V/Å. (2) Gies and Gerhardts[6] have studied the penetration of intense electric fields into the surface of a rigid jellium, via a self-consistent calculation of the centroid $\bar{x}$ of induced surface charge. Their prediction of nonlinear field dependence of $\bar{x}$ for fields less than ~ 5 V/Å is corroborated by our work. They also found asymptotic linearity of $\bar{x}$ with F for $F \gtrsim 10$ V/Å due to rigid displacement of the "saturated" electron-density profile. For these large fields, and even for the more moderate fields less than F_c, our work indicates that field-driven surface-layer displacements are important, and must therefore be included in metal-surface–intense-field calculations.

ACKNOWLEDGMENT

This work was supported in part by the National Science Foundation under Grants No. DMR-80-16117 and No. DMR-84-20964.

APPENDIX: JELLIUM PHONON FREQUENCIES

We seek a general expression for the bulk longitudinal phonon frequencies ω_k of the jellium metal. Consider a right cylindrical sample with uniform cross section A normal to the longitudinal (x) axis. The sample is subdivided into N rigid sections of width d by planes at $x=ld$, $l=1,2,3,\ldots,N-1$, like a loaf of sliced bread. Each section has a mass $M=\rho Ad$, where ρ is the mass density of the metal. A small-amplitude longitudinal phonon of wave vector $\mathbf{k}(k_x=k)$ will create a change $\delta n_+(x)$ in the positive background charge localized in the regions near $x=ld$. The electronic charge will respond to $\delta n_+(x)$ and the crystal energy will change by an amount δE. We take N very large and impose periodic boundary conditions on the system.

Following Vosko *et al.*,[19] the longitudinal phonon frequencies ω_k of the sectioned jellium metal are obtained in the harmonic approximation from the dynamical matrix D as

$$\omega_k^2 = D(k) = M^{-1}\sum_l \Phi(l)\exp(-ikld) ,$$

where

$$\delta E = \tfrac{1}{2}\sum_{l,l'}\{\partial^2 E/\partial u_l \partial u_{l'}\}_0 u_l u_{l'}$$
$$= \tfrac{1}{2}\sum_{l,l'}\Phi(l-l')u_l u_{l'}$$

is the second-order change in energy when each lth section of the positive background charge is displaced by u_l from its equilibrium position. The energy change δE may be found from the work of Perdew and Datta[20] on charge density waves in jellium. The result is

$$\omega_k^2 = (8\pi\bar{n}^2/\rho d^2)\sum_G (k+G)^{-2}[1-\cos(k+G)d] \times F(\bar{n},|k+G|) ,$$

where $G=\text{integer}\times 2\pi/d$ is a reciprocal-lattice vector. In this expression, all quantities are in atomic units ($\hbar=m=e^2=1$) and

$$F(\bar{n},q) = 1+(4\pi/q^2)\Pi_0(\bar{n},q)/\bar{\epsilon}(q) ,$$

where

$$\bar{\epsilon}(q) = 1-(4\pi/q^2)\{1-G(q)\}\Pi_0(\bar{n},q) ,$$

$$\Pi_0(\bar{n},q) = (-k_F/\pi^2) \times \{\tfrac{1}{2}+[(1-x^2)/4x]\ln|(1+x)/(1-x)|\} ,$$

$$x = q/2k_F ,$$

and

$$G(q) = (-q^2/4\pi)(\partial^2/\partial n^2)[n\,\epsilon_{\rm xc}(n)]\,|_{n=\bar{n}}$$

in the local-density approximation.

*Present address: Delgado Community College, New Orleans, LA 70119.

[1]A. K. Theophilou, J. Phys. F **2**, 1124 (1972).
[2]A. K. Theophilou and A. Modinos, Phys. Rev. B **6**, 801 (1972).
[3]N. D. Lang and W. Kohn, Phys. Rev. B **1**, 4555 (1970); **3**, 1215 (1971).
[4]R. Monnier, J. P. Perdew, D. C. Langreth, and J. W. Wilkins, Phys. Rev. B **18**, 656 (1978).
[5]A. Kiejna, Solid State Commun. **50**, 349 (1984).
[6]P. Gies and R. R. Gerhardts, Phys. Rev. B **31**, 6843 (1985); **33**, 982 (1986).
[7]L. M. Kahn and S. C. Ying, Surf. Sci. **59**, 333 (1976).
[8]E. R. McMullen, J. P. Perdew, and J. H. Rose, Solid State Commun. **44**, 945 (1982); E. R. McMullen, Ph.D. thesis, Tulane University, 1985.
[9]E. W. Müller and T. T. Tsong, *Field Ion Microscopy: Principles and Applications* (Elsevier, New York, 1969).
[10]P. Hohenberg and W. Kohn, Phys. Rev. **136**, B864 (1964); W. Kohn and L. J. Sham, *ibid.* **140**, A1133 (1965).
[11]R. Monnier and J. P. Perdew, Phys. Rev. B **17**, 2595 (1978).
[12]A. Sugiyama, J. Phys. Soc. Jpn. **15**, 965 (1969); D. C. Langreth, Phys. Rev. B **5**, 2842 (1972). See also Ref. 4.
[13]J. P. Perdew and A. Zunger, Phys. Rev. B **23**, 5048 (1981).
[14]D. M. Ceperley, Phys. Rev. B **18**, 3126 (1978); D. M. Ceperley and B. J. Adler, Phys. Rev. Lett. **45**, 566 (1980).
[15]I. N. Levine, *Quantum Chemistry,* 2nd ed. (Allyn and Bacon, Boston, 1974).
[16]F. K. Schulte, Surf. Sci. **55**, 427 (1976).
[17](a) J. Ferrante and J. R. Smith, Phys. Rev. B **19**, 3911 (1979); (b) J. H. Rose, J. Ferrante, and J. R. Smith, Phys. Rev. Lett. **47**, 675 (1981); (c) J. R. Smith, J. Ferrante, and J. H. Rose, Phys. Rev. B **25**, 1419 (1982); (d) J. H. Rose, J. R. Smith, and J. Ferrante, *ibid.* **28**, 1835 (1983).
[18]J. P. Perdew and R. Monnier, J. Phys. F **10**, L287 (1980); J. P. Perdew, Phys. Rev. B **25**, 6291 (1982); R. N. Barnett, U. Landman, and C. L. Cleveland, *ibid.* **28**, 1685 (1983); K.-P. Bohnen, Surf. Sci. **147**, 304 (1984); K. M. Ho and K.-P. Bohnen, Phys. Rev. B **32**, 3446 (1985).
[19]S. H. Vosko, R. Taylor, and G. H. Keech, Can. J. Phys. **43**, 1187 (1965).
[20]J. P. Perdew and T. Datta, Phys. Status Solidi B **102**, 283 (1980).
[21]E. Zaremba, Solid State Commun. **23**, 347 (1977).